Antifreeze glycopeptide adsorption on single crystal ice surfaces using ellipsometry

P. W. Wilson,* D. Beaglehole,* and A. L. DeVries‡

*Physics Department, Victoria University of Wellington, Wellington, New Zealand; and ‡Department of Physiology and Biophysics, University of Illinois, Urbana-Champaign, USA

ABSTRACT Antarctic fishes synthesise antifreeze proteins which can effectively inhibit the growth of ice crystals. The mechanism relies on adsorption of these proteins to the ice surface. Ellipsometry has been used to quantify glycopeptide antifreeze adsorption to the basal and prism faces of single ice crystals. The rate of accumulation was determined as a function of time and at concentrations between 0.0005 and 1.2 mg/ml. Estimates of packing density at saturation coverage have been made for the basal and prism faces.

1. INTRODUCTION

Many polar fishes synthesise antifreeze proteins (AFs) which lower the freezing point of their body fluids a few tenths of a degree below the freezing point (−1.9°C) of seawater. In the Antarctic notothenioid fishes and in some northern cods the AF's are glycopeptides, while in the bipolar zooarcid fishes, some northern flat fishes and sculpins they are peptides (1–4). These AF's lower the freezing point via a non-colligative process and therefore make only a negligible contribution to the osmotic concentration of the fishes' body fluids. At physiological concentrations (35 mg/ml), they inhibit the growth of endogenous ice crystals to temperatures 1.4°C below the equilibrium freezing point (melting point) which for blood is −1°C (1). This separation of the freezing process and the equilibrium freezing point has often been referred to as thermal hysteresis and is characteristic of the AF's. It also occurs in aqueous solutions of purified antifreeze.

Although the exact mechanism of the freezing inhibition has not been ellucidated, it has clearly been demonstrated that with all of the various AF's adsorption to ice is involved (5), and it has recently been shown that the adsorption to ice crystal faces is antifreeze specific and in many cases completely inhibits growth on those faces (6). Although adsorption is important it is not known exactly how adsorption inhibits growth on the adsorption plane. It has been proposed that adsorption of AF's to the growth faces divides them into many small fronts which have a high surface area to volume ratio. This increase in surface free energy is thought to produce a local depression of the freezing point (the Kelvin effect). Although adsorption is crystal plane specific (6) and the antifreeze hysteretic effect saturates between at 35 and 40 mg/ml, it is not known how much AF is adsorbed to the adsorption planes of ice.

This paper describes a quantitative study of the adsorption of antifreeze glycopeptides to the basal and prism faces of single ice crystals using ellipsometry.

Address correspondence to P. Wilson, Physics Department, Victoria University of Wellington, P.O. Box 600, Wellington, New Zealand.

1.1 Antifreeze glycopeptides

Antifreeze glycopeptides (AFGPs) are present in at least eight distinct sizes in the antarctic notothenioid fishes ranging in molecular weight from 2,600–34,000 D. The different sizes are composed of repeats of the glycotripeptide, ala-ala-thr with the disaccharide, galactosyl-*N*-acetylgalactosamine glycosidically linked to each threonine (7). In contrast to the large AFGP's the small ones, 7 and 8 have prolines substituted for alanine at positions 7, 10, and 13. The larger fractions (AFGP 1–5) have a greater freezing point depression activity than the smaller fractions (AFGP 7, 8) (8). Their basic structure is thought to be a three-fold left-handed helix (9), with a diameter of 8 or 9 Å (5) and lengths ranging between ~40 and 400 Å. The repeating hydrophilic carbohydrate side chains appear on one side of the molecule while most of the methyl groups of the alanine side chains are located on the other side, and this amphiphilicity is thought to be important for strong binding of the AFGP's to the ice surface (6, 10).

1.2 Adsorption to ice

Recent reviews of the various models put forward to explain the antifreeze mechanism have been given by Avanov (11), Knight et al. (6), Hew and Yang (12) and Wilson (13). The first detailed model proposed for the mechanism of action of these AF's is that of Raymond and DeVries (5), who termed it adsorption-inhibition (AI). It was proposed that AF molecules hydrogen-bond to the ice lattice and cause ice steps to grow between adsorbed molecules.

Direct evidence for AF adsorption to ice has come from diverse experiments, including the following: (*a*) Using surface enhanced second harmonic generation (SSHG), Brown et al. (14) showed that adsorption of AF occurs at the ice surface. Adsorption causes inversion asymmetry which is detectable by SSHG. Their results were not ice crystal-face specific and the intensity of the second harmonic signal did not appear to saturate with increasing AF concentration (to 100 mg/ml).

(*b*) Recent experiments by Knight et al. (6, 15) have

0006-3495/93/06/1878/07 $2.00

been able to show particular adsorption planes for various peptide and glycopeptide AFs. By growing hemispherical, single ice crystals and observing etch patterns produced by preferentially-adsorbed dilute AF solutions, they found particular types of AF bound to specific crystal planes. They reported that they AFGP 7, 8 bind to the primary prism planes ($10\bar{1}0$). Their results showed that low concentrations (0.03 mg/ml) the AF's become adsorbed to and incorporated into specific ice faces. It has also been reported that AFGP 1–5 bind to the ($41\bar{5}0$) plane for concentrations less than 0.03 mg/ml, changing to the ($10\bar{1}0$) plane at higher concentrations (C. Knight, NCAR, personal communication).

1.3 Ice crystal habits in the presence of AF

Raymond et al. (16) report that single ice crystals suspended in AFGP 1–5 solutions at temperatures within the hysteresis gap formed hexagonal pits on the basal plane. The flat surface of the basal plane diminished during *c*-axis growth, which then stopped when the basal plane was completely transformed into a pitted surface. In contrast, in the presence of AFGP 7 and 8, *c*-axis growth occurred to a greater extent and the edges of the basal plane formed bipyramidal faces. Growth at any temperature within the hysteresis gap resulted in the crystal taking the shape of a hexagonal bipyramid and once complete no further growth could be detected.

2. CRYSTAL GROWTH

In the experiments described here single ice crystals were grown by slow freezing from the surface of a well-insulated bucket with 3 liters of distilled, deionized water. Identification of the crystal boundaries and the basal plane was by crossed-polaroids. Determination of the crystal axes for prism interface experiments was by observation of Tyndall flowers produced within the crystals by radiation with a 1,000 W quartz-halogen lamp. This radiation also caused liquid water to force grain boundaries apart, and the frozen slab to separate into the individual crystals. Single seed crystals (~10 mm cubes) were then cut and mounted in the ellipsometer cell on the cold stub (see Fig. 1). Distilled, deionized water at +0.05°C was then introduced to the cell and the temperature lowered via the cold stub. In this way heat transfer was through the crystal, which grew to fill the cell to the desired height. The rate of growth was set at ~0.5 mm/h until the ice-water interface was at the correct height, when the thermal gradient was set at 1 or 2°C/mm, perpendicular to the interface. This relatively large gradient was required to keep the surface flat and so aid in reflecting light specularly into the detector. The interface could be raised and lowered by careful control of the current to both the Peltier device and the nichrome wire heater at the top of the liquid level. To achieve this the overall

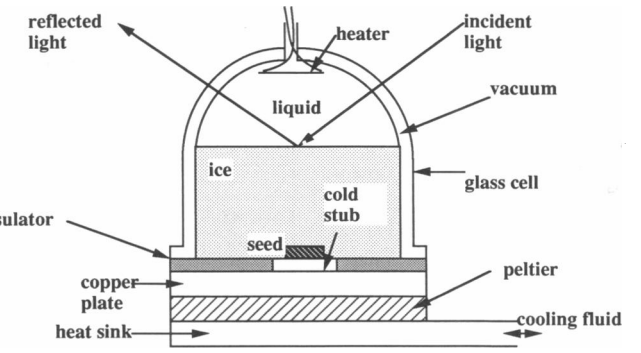

FIGURE 1 The ellipsometer cell consisted of a double-walled glass hemisphere mounted on a cold stub. Vacuum between the walls acted as an insulator to reduce condensation. The ice/water interface could be maintained at the desired height by controlling the Peltier and heater currents. Heat removed from the liquid via the cold stub ensured single crystal growth with orientation set by the positioning of the seed crystal. The glass was annealed to reduce strain and hence unwanted birefringence. Solutions were added to the water above the ice by passing a syringe needle through the same tube as the heater wires.

temperature gradient was held constant and both currents altered to move the interface, which could be maintained at the center of curvature of the glass over extended periods. (It is desirable for the incident and reflected light to meet the glass of the cell wall at normal incidence). At the end of each experiment the ice was removed and checked for orientational integrity and crystal singularity.

3. MEASUREMENT OF ADSORPTION BY ELLIPSOMETRY

Ellipsometry determines the state of polarization of light reflected from an interface, and is a sensitive tool for the analysis of surface adsorbants. The optical properties of two phases separated by an interface will in general be different, and in the transition region between the phases, departure of the dielectric constant (or refractive index) profile from a sharp step-type interface induces a small component of circular polarisation. This can be studied by measuring the ratio r, $r = r_p/r_s$, where r_p and r_s are the p and s wave reflection amplitudes. Circular polarisation causes this ratio to be complex $r = Re(r) + iIm(r)$. At the Brewster angle θ_B, $Re(r, \theta_B) = 0$, and $\bar{\rho} = Im(r, \theta_B)$ is directly proportional to departures from the step profile. $\bar{\rho}$ is called the coefficient of ellipticity, or ellipticity for short. Measurements of ellipticity provide both the magnitude and sign of $\bar{\rho}$, and the sign in particular can be very useful in identifying an appropriate model for the transition region, as we shall see.

Water is optically isotropic, but ice is weakly anisotropic, and this anisotropy extends into the transition region between the phases (Beaglehole and Wilson, 1992, in preparation). With axes z normal to the interface, and x lying in the plane of incidence, $\bar{\rho}$ for an anisotropic

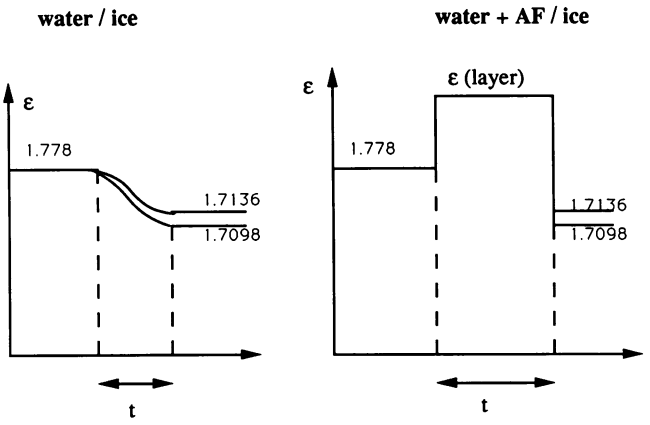

FIGURE 2 (*a*) In a pure water system the dielectric constant varies continuously between bulk ice and water, and can be modelled by a tanh profile. (*b*) A model for adsorbed AF with dielectric constant $\varepsilon > \varepsilon_1, \varepsilon_2$.

transition region of dielectric constant ε_x, ε_z lying between an incident isotropic medium with dielectric constant ε_1 and an anisotropic medium of dielectric constant ε_{2x}, ε_{2z} for thin transition regions is

$$\bar{\rho} = \frac{\pi}{\lambda} \frac{(\varepsilon_1 + \varepsilon_{2x})}{(\varepsilon_{2z} - \varepsilon_1)^{1/2}} \frac{1}{(\varepsilon_{2x}\varepsilon_{2z} - \varepsilon_1^2)} \eta \qquad (1)$$

with

$$\eta = -\int dz \left\{ \frac{(\varepsilon_{2x}\varepsilon_{2z} - \varepsilon_1^2)}{(\varepsilon_{2x} - \varepsilon_1)} - \frac{(\varepsilon_{2z} - \varepsilon_1)}{(\varepsilon_{2x} - \varepsilon_1)} \varepsilon_x - \frac{\varepsilon_{2x}\varepsilon_1}{\varepsilon_z} \right\}. \qquad (2)$$

The transition region in a one component system is often modelled by a continuous profile characterised by a thickness δ, where the properties of the interface vary smoothly from one side of the interface to the other, see Figure 2. A tanh profile uses (neglecting interface anisotropy)

$$\varepsilon(z) = \frac{(\varepsilon_1 + \varepsilon_2)}{2} + \frac{(\varepsilon_1 - \varepsilon_2)}{2} \tanh(z/2\delta). \qquad (3)$$

For light incident from water to ice $\varepsilon_1 > \varepsilon > \varepsilon_2$, so that η and hence $\bar{\rho}$ are negative. However, if a layer of AF adsorbs to the ice surface, a model in which $\varepsilon(z)$ steps between the ice and water value is more appropriate, Fig. 2, and in this case η and $\bar{\rho}$ are positive, $\varepsilon(z) > \varepsilon_1, \varepsilon_2$.

The birefringence modulation ellipsometer has been utilized extensively by Beaglehole to study the ice-vapour interface (17) and more recently vapour-adsorption on solid surfaces (see for instance, see reference 18). The ellipsometer produces signals which are directly proportional to the real and imaginary parts of the complex reflectivity ratio r; the ellipsometer automatically finds the Brewster angle by driving the angles of incidence and reflection until a zero in the $Re(r)$ is obtained.

The dielectric constants used for ice take into account anisotropy and based upon Furukawa et al. (19) are Basal plane: $\varepsilon_{2x} = 1.7136$, $\varepsilon_{2z} = 1.7098$ Prism plane: ε_{2x} varies between 1.7098 and 1.7136, average value 1.7117, $\varepsilon_{2z} = 1.7136$. The value for ε_1 used for the water (at 5,500 Å) is 1.7780.

Inserting these values into the expression above gives for the basal plane $\bar{\rho} = -0.0159\eta$, and for the prism plane $\bar{\rho} = -0.0164\eta$ (with η in Å units).

4. THE ICE-WATER INTERFACE

In modeling the adsorption of AF to the surface of ice it has been common to consider the ice-water interface to be smooth and well defined (see for example reference 10). The transition from ice to water is, in fact, more gradual, but to date only theoretical estimates rather than measurements of its thickness have been available (20). The ellipticity of the ice-water interface was measured for each crystal before the antifreeze was introduced into the water phase. It was found to be consistently small and negative, and differed systematically between prism-water and basal-water interfaces, having an average value of -0.0014 ± 0.0005 for the prism face, and -0.001 ± 0.0007 for the basal face. The interpretation of this data including effects of interface anisotropy in a continuous transition region is discussed in another paper (Beaglehole and Wilson, in preparation); briefly, the data support a model of the transition region with a 10–90% thickness of ~2 nm, i.e., the distance over which the dielectric constant varies from 10 to 90% of the value difference (21). Results strongly indicate preferential molecular alignment in the transition region.

5. ADSORPTION AT THE PRISM FACE

In the following experiments and discussions AFGP 1–5 refers to a mixture of the five heaviest glycopeptides, and AFGP 7, 8 describes a mixture of the two lightest, while AFGP 8, describes the lightest alone. The glycopeptide antifreezes were isolated from blood serum of the Antarctic notothenid *Dissostichus mawsoni* by DEAE ion-exchange chromatography. Freeze-dried, purified protein was dissolved in distilled, deionized water (conductivity > 18 MΩ cm) to the various concentrations used. We report here only glycopeptide adsorption. Work with peptides will be published in the future.

Once $\bar{\rho}$ was measured for the pure ice-water interface, 0.1 ml of aqueous AF at a concentration, c and at 0°C was added by syringe to the 4 ml water above the ice. Concentrations given below were calculated as total AF (mg) per 4.1 ml of water. In each case the AF solution was added to the water 2 mm below the surface and allowed to diffuse to the interface. After several minutes $\bar{\rho}$ changed to a positive value substantially larger than the initial negative value for the ice-water interface. This variation in $\bar{\rho}$ was thus consistent with that expected for AF adsorption. From this change, the change $\Delta\eta$ due to the AF adsorption was found. Fig. 3 shows typical time

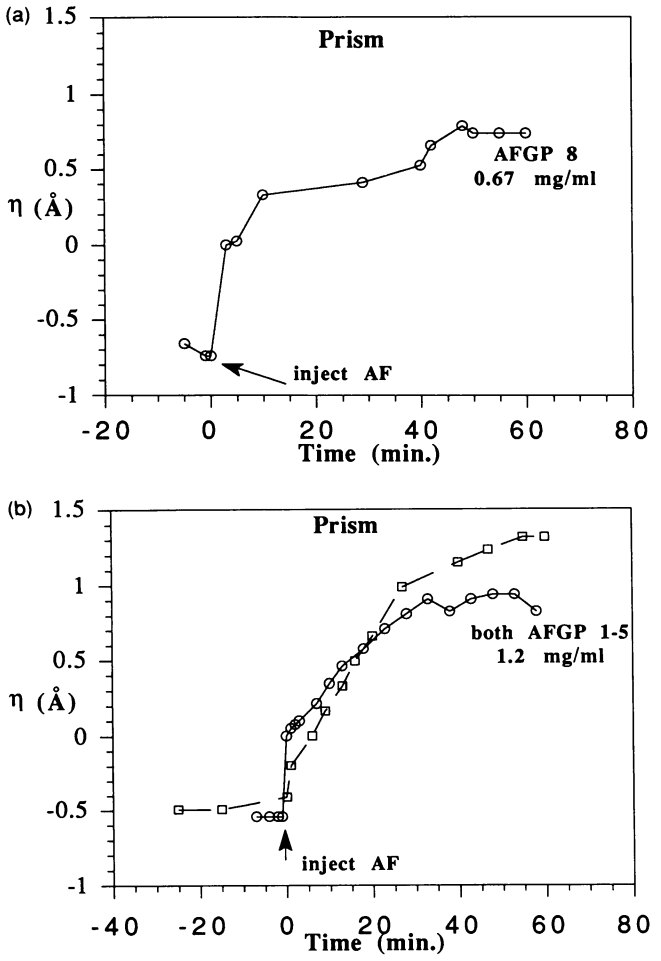

FIGURE 3 (*a*) Adsorption of AFGP 8 onto the prism plane as a function of time. Concentration was 0.675 mg/ml after addition to the water above the ice. The negative $\bar{\rho}$ signal changed sign when AF was added at time $t = 0$, and saturated as time progressed. Monitoring the signal for longer time periods (15 h) showed that the AF did not desorb, and there was no measurable ice growth at the interface. (*b*) Adsorption of AFGP 1–5 onto the prism plane for two different crystals, both with AF added at 1.2 mg/ml. Again, no desorption was seen and the antifreeze effectively halted the interface growth, and the surface remained smooth.

dependence curves for adsorption of AFGP 8 and AFGP 1–5 on the prism plane. These time periods are similar to published adsorption curves for proteins at inorganic surfaces (22, 23). The signal remained steady for at least the longest observation time of 15 h, indicating saturation coverage.

There was some variation in the change in $\bar{\rho}$ between crystals, larger than the instrumental error in $\bar{\rho}$ of ± 0.0002. The variation has been attributed to the optical alignment, which varied in each case since the reflecting surfaces were not perfectly horizontal or flat. The weak intensity of light reflected from the ice-water interface made optical alignment difficult. For low concentration solutions the alignment was even more difficult, since the interface tended to grow or recede at rates of at least 100 μm/h. It was found that higher concentrations of AF helped to stabilize the interface, allowing the measurement of $\bar{\rho}$ over longer periods.

When plotted as a function of concentration, see Fig. 4, $\Delta\eta$ was found to increase and level off at approximately 0.35 Å, for concentrations greater than 0.2 mg/ml. This appears to be a typical adsorption isotherm (23). There was little difference between AFGP 1–5 and AFGP 8. In all cases the ice surface remained smooth, and no pitting was observed.

Knight has suggested that at low concentrations the $(41\bar{5}0)$ faces have a higher preference for AFGP 1–5 adsorption than the $(10\bar{1}0)$ faces, so the former perhaps would have a higher saturation adsorption than some of the values we are reporting here.

6. ADSORPTION AT THE BASAL FACE

In all cases when the AFGPs were added to the water above the basal face, $\bar{\rho}$ changed sign, as it did for the prism face above, but surface roughening then occurred.

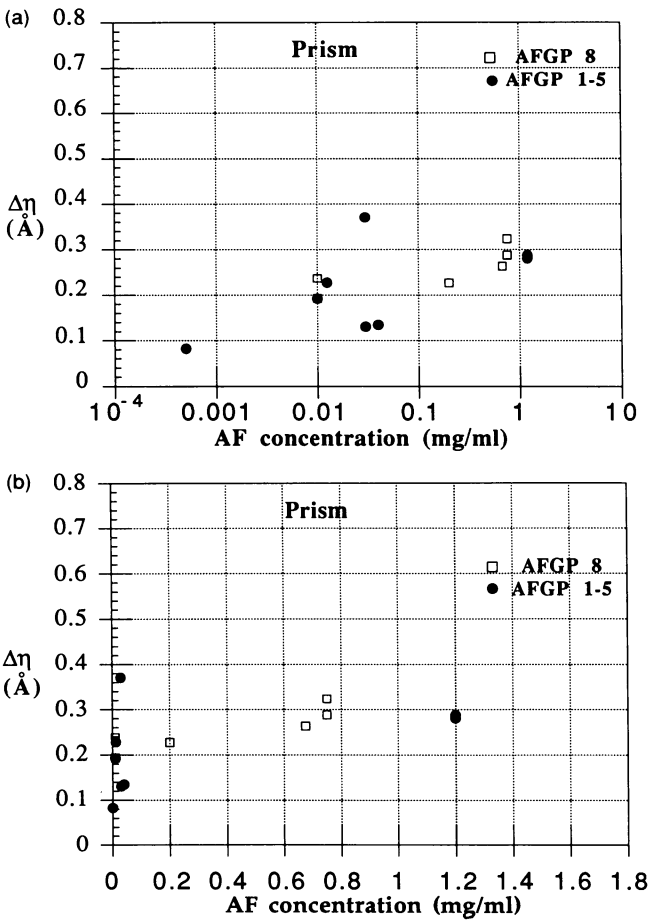

FIGURE 4 Prism plane adsorption as a function of concentration, (*a*) on a logarithmic concentration scale, (*b*) on a linear scale. We see a general trend towards greater $\Delta\eta$ values with increasing concentration of both AFGP 1–5 and AFGP 8. Saturation occurs above ~0.2 mg/ml AF concentration for both AFGP 8 and AFGP 1–5.

With AFGP 1–5 the surface formed visible pits. These pits were similar to, but not as deep as, those described by Raymond et al. (16), probably because the temperature gradient across the interface would limit the region of growth.

With AFGP 8, there was a trend for $\Delta\eta$ to increase with concentration, see Fig. 5. The time for roughening to occur was directly related to concentration, being from about one hour to just one minute for higher concentration solutions. The surface-roughening produced diffuse reflection of the light beam, and the specular component became too weak to measure. We were thus unable to determine whether adsorption was complete before measurements were forced to cease. The observed roughness with AFGP 8 did not appear to be the pitting observed with AFGP 1–5, but rather a whitening of the surface, perhaps pitting on a smaller scale. It also did not

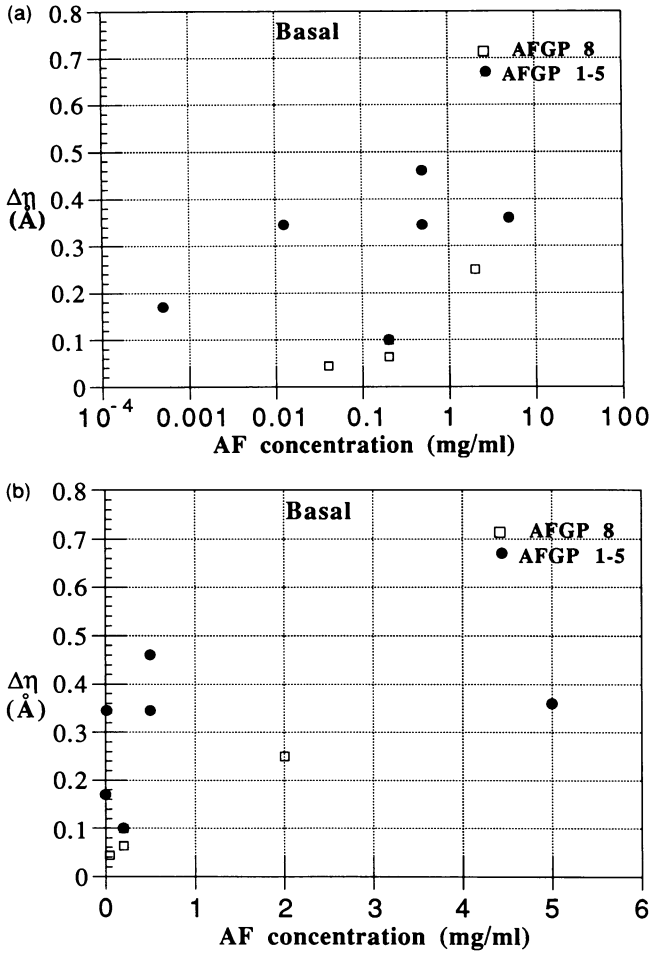

FIGURE 5 Basal plane adsorption as a function of AF concentration, (*a*) on a logarithmic scale, and (*b*) a linear scale. In the case of AFGP 8 the adsorption parameter, $\Delta\eta$, increased with concentration and was detectable in each case until the basal surface became too rough to specularly reflect the incident light. The AFGP 1–5 adsorption was difficult to measure due to the growth of pits in the basal surface, reducing the specularly reflected light. The adsorption isotherm appears to be near saturation ~1–2 mg/ml.

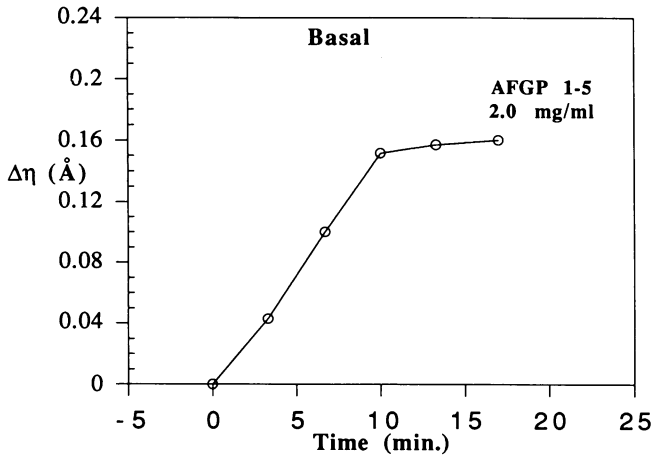

FIGURE 6 Using a larger thermal gradient ensured the pits formed following injection of AF were very shallow, and on one occasion when the basal plane showed only a low density of pits, the adsorption AFGP 1–5 to saturation was observed.

lead to the pyramidal growth previously reported for AFGP 7, 8 at the basal plane (16). Our high temperature gradient probably inhibits large scale crystal growth.

There was no detectable time delay between the adsorption signal and the onset of surface roughening.

It was possible with AFPG 1–5 to limit the height of the surface roughness by increasing the thermal gradient. On one occasion when the gradient was doubled this resulted in sufficient specular reflection for the measurement of $\bar{\rho}$ to proceed until saturation. The surface had few hexagonal pits visible, with only four covering ~50% of the light spot area (~25 mm^2). The spaces between pits were flat and smooth; steps were visible on the inside walls of the pits. As can be seen from the curve in Fig. 6 adsorption was evident, which saturated at $\Delta\eta$ values similar to those found at the prism planes. Since only horizontal basal surfaces would reflect light into the detector at the Brewster angle, the observed signal implies adsorption to the basal plane. The suggestion by Raymond et al. (16) that the sites for initialization of pitting are lattice dislocations or defects remains a matter of conjecture.

7. DISCUSSION

A schematic representation of adsorbed AF is shown in Fig. 7. Sub-monolayer coverage implies lower packing density at the ice surface. Any adsorbed layer will have a dielectric constant approaching, but less than that of 100% AF. The latter value is not known, but we have attempted to estimate it in the following ways: (*a*) The ellipticity of the water-air interface was measured for dilute AF solutions. It is very common for organics to form a monolayer at the water surface, and amphiphilic molecules such as these AF's are thought to be no exception (24). When solutions containing AFGP 8 at 0.1 mg/ml

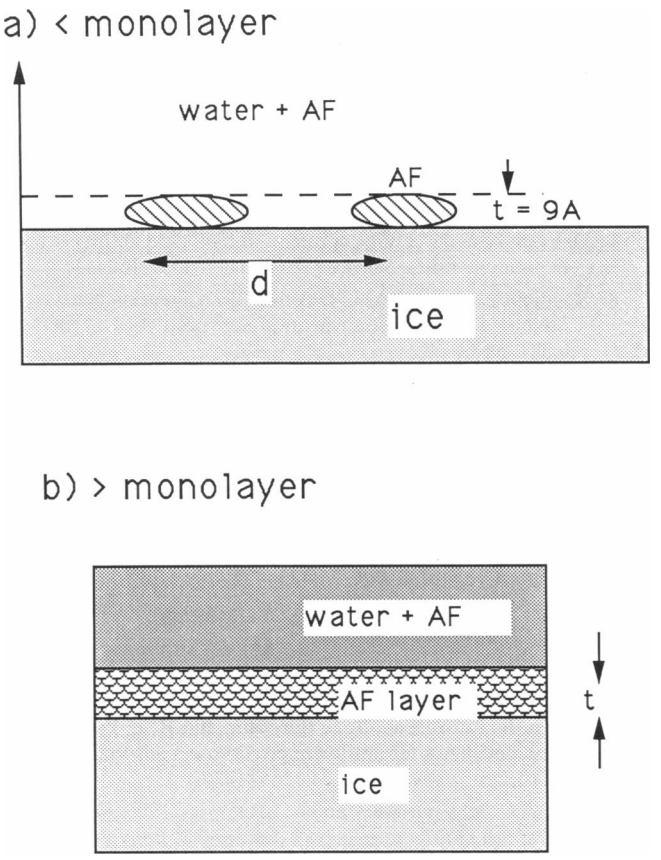

FIGURE 7 Sub-monolayer coverage is depicted by a larger spacing, d, between adsorbed molecules since the molecules have a minimum diameter, t.

were examined in this way, $\bar{\rho}$ was found to be 0.0033 ± 0.0005. This corresponds to a dielectric constant ε of 2.3 ± 0.1 when a layer thickness of 9 Å is used, corresponding to the diameter of the cylindrical AF molecules. When AFGP 1–5 was measured in the same way, $\bar{\rho}$ was measured to be 0.0049, with $\varepsilon \sim 2.5 \pm 0.1$ using the same 9 Å estimate for the layer thickness. A lower packing density for the longer molecules could explain this difference in ε.

(*b*) The refractive index n for aqueous AF solutions of up to 40 mg/ml was measured with an Abbe refractometer. The following expression was used to estimate $\varepsilon = n^2$ for 100% solution:

$$3(\varepsilon - 1)/(\varepsilon + 2) = (p_1 + p_2)/\varepsilon_0 \qquad (4)$$

Here p_1 and p_2 are the polarization per unit volume contributed by AF and water, respectively, which may be written $p_1 = cp'$, $p_2 = (1 - c)p''$, with c and $(1 - c)$ the volume fractions of each component, p' and p'' the polarization density of the two pure components. The properties of water are known; a density for pure AF is needed to convert the AF concentration in mg/ml to c. Using densities for AF of 1.3 to 1.5 g/ml respectively we found that ε ranges between 2.28 and 2.37, these values being based upon those of proteins of similar size and configuration.

Considering these various estimates and uncertainties, we have chosen to use $\varepsilon \sim 2.33$ in the following calculations of adsorbed layer thicknesses. The values for $\Delta\eta$ can be related to a layer thickness t by the integral in Eq. 2. For the basal plane we obtain $\Delta\eta = 0.18\ t$, for the prism plane $\Delta\eta = 0.13\ t$. Using the saturation values for $\Delta\eta$ from Figs. 4 and 5 of 0.25 to 0.35 Å, gives saturation thicknesses t of 1.4 and 2.7 Å for the basal and prism planes respectively, corresponding to saturation coverages of 0.16 to 0.3 of a monolayer.

Some of the uncertainties in the estimate of the saturation coverage can be removed by comparing directly the water-air ellipticities with the water-ice ellipticities. The ratio of the saturation coverages of the basal and prism faces respectively to those at the water-air surface are 0.2 ± .05 and 0.44 ± .15, the range in these values spanning ε values between 2 and 2.4.

Chou et al. (25) have proposed that $\varepsilon \sim 2$ for polypeptides surrounded by polar molecules. This value leads to saturation thicknesses of 5.5 and 14 Å for the basal and prism faces, respectively, closer to a monolayer at saturation.

Using these experimental fractional monolayer coverages it is possible to estimate the average distance separating adsorbed molecules if some assumptions are made regarding the surface area taken up by each adsorbed molecule.

The molecular dimensions given earlier suggest the surface area occupied by single AFGP molecules ranges from 4,400 Å^2 (AFGP 1) to 350 Å^2 (AFGP 8) if the molecule is fully extended. Knight et al. (15) suggest that the heads and tails of the longer glycopeptides may not adsorb but be suspended in solution. However, we consider these values to be the minimum space taken up by an adsorbed molecule. Ahmed et al. (26) used quasi-elastic light scattering to determine the effective hydrodynamic radius of solutions of AFGP 4 and AFGP 8, reporting values of 30 Å and 12 Å, respectively. Using the same volumes but flattening the molecules to 9 Å corresponds to surface areas of 3,000 Å^2 and 200 Å^2 for AFGPs 4 and 8, similar to the values above.

From these estimates of the covered surface area, we estimate that the average distance between adsorbed molecules ranges between 50 Å (AFGP 8) and 165 Å (AFGP 1) on the basal face and 33 Å (AFGP 8) and 120 Å (AFGP 1) on the prism face. If the molecules are aligned at the ice surface, as suggested by the lattice-match argument (1, 3, 6) it would be possible to have greater packing densities than those estimated here.

Knowledge of the distance between adsorbed molecules has implications in the model for ice growth inhibition by the Kelvin effect. The latest model, proposed by Knight et al. (6), describes growth of ice between AF molecules pinned at the ice surface, resulting in convex distortions of the interface (described as "felting") (a

requirement for freezing point depression by the Kelvin effect). The model requires that the working temperature is above the ice roughening transition, allowing curvature at the interface as opposed to stepwise growth. In a recent discussion of this model (13) it was shown that for particular molecular spacings the height of the interface distortions could be calculated at any value of nonequilibrium freezing point depression. If the molecular spacings given above are used in that model we find that the interface distortions vary in height between 17 Å (AFGP 1) and 1.5 Å (AFGP 8), assuming a freezing point depression of 1°C. It is worth pointing out that for a given distortion height the maximum spacing between adsorbed molecules determines the minimum ΔT and so the overall nonequilibrium freezing point. In reference 13, it was argued that the maximum height of ice extending into solution (growing between adsorbed molecules) should be comparable to the AF molecular diameter (t = 9 Å for glycopeptides).

8. SUMMARY

Our results indicate a surface density of AFGP about one-half that at the air-water interface for the prims face, which is constant above AF concentrations of about 0.2 mg/ml. The basal face shows a surface density about one-half that of the prism face. We estimate that for the basal and prism planes respectively saturation coverages are 0.16 to 0.3 of a monolayer.

Hew and Yang (12) point out that Raymond and DeVries (5) failed to consider the concentration dependence of the distribution coefficient of AF on the ice surface. Our constant adsorption above 0.2 mg/ml suggests that this is not an important consideration.

The observed saturation coverages are reasonably consistent with those predicted by the freezing point depression caused by the Kelvin surface curvature effect.

This work was supported in part by NSF DPP 87-16296 to A. L. Devries.

Received for publication 1 October 1992 and in final form 28 January 1993.

REFERENCES

1. DeVries, A. L. 1984. Role of glycopeptides and peptides in inhibition of crystallization of water in polar fishes. *Phil. Trans. R. Soc. Lond.* B304:575–588.
2. DeVries, A. L. 1988. The role of antifreeze glycopeptides and peptides in the freezing avoidance of Antarctic fishes. *Comp. Biochem. Physiol.* 90B:611–621.
3. Cheng, C. C., and A. L. DeVries. 1991. The role of antifreeze glycopeptides and peptides in the freezing avoidance of cold-water fish. *In* Life Under Extreme Conditions. Guido di Prisco, editor. Springer-Verlag Berlin, Heidelberg. 1–14.
4. Davies, P. L., and C. L. Hew. 1990. Biochemistry of fish antifreeze proteins. *FASEB J.* 4:2460–2468.
5. Raymond, J. A., and A. L. DeVries. 1977. Adsorption inhibition as a mechanism of freezing resistance in polar fishes. *Proc. Natl. Acad. Sci. USA.* 74:6, 2589–2593.
6. Knight, C. A., C. C. Cheng, and A. L. DeVries. 1991. Adsorption of a-helical antifreeze peptides on specific ice crystal surface planes. *Biophys. J.* 59:409–418.
7. DeVries, A. L. 1971. Glycoproteins as biological antifreeze agents in antarctic fishes. *Science (Wash. DC).* 172:1152–1155.
8. Raymond, J. A., and A. L. DeVries. 1972. Freezing behaviour of fish blood glycoproteins with antifreeze properties. *Cryobiology.* 9:541–547.
9. Rao, B. N. N., and C. A. Bush. 1987. Comparison by H'-NMR spectroscopy of the 2600 Dalton antifreeze glycopeptide of polar cod with that of the high molecular weight antifreeze glycoprotein. *Biopolymers.* 26:1227–1244.
10. Chou, K-C. 1992. Energy-optimized structure of antifreeze protein and its binding mechanism. *J. Mol. Biol.* 223:509–517.
11. Avanov, A. Y. 1990. Biological antifreezes and the mechanism of their activity. *Mol. Biol.* 24:473–487.
12. Hew, C. L., and D. S. C. Yang. 1992. Protein interaction with ice. *Eur. J. Biochem.* 203:33–42.
13. Wilson, P. W. 1993. Explaining thermal hysteresis by the Kelvin effect. *Cryoletters.* 14:31–36.
14. Brown, R. A., Y. Yeh, T. S. Burcham, and R. E. Feeney. 1986. Direct evidence for antifreeze glycoprotein adsorption onto an ice surface. *Biopolymers.* 24:1265–1270.
15. Knight, C. A., E. Driggers, and A. L. DeVries. 1993. Adsorption to ice of fish antifreeze glycopeptides 7 and 8. *Biophys. J.* 64:252–259.
16. Raymond, J. A., P. W. Wilson, and A. L. DeVries. 1989. Inhibition of growth of nonbasal planes by fish antifreezes. *Proc. Natl. Acad. Sci. USA.* 86:881–885.
17. Beaglehole, D. 1980. Ellipsometric study of the surface of simple liquids. *Physica.* 100B:163–174.
18. Beaglehole, D., and H. K. Christenson. 1992. Vapour adsorption on mica and silicon-entropy effects, layering and surface forces. *J. Phys. Chem.* 96:3395–3403.
19. Furukawa, Y., M. Yamamoto, and T. Kuroda. 1987. Ellipsometric study of the transition layer on the surface of an ice crystal. *J. Crystal Growth.* 82:665–667.
20. Karim, O. A., and A. D. J. Haymet. 1988. The ice/water interface: a molecular dynamics simulation study. *J. Chem. Phys.* 89:11, 6889–6896.
21. Lekner, J. 1983. Anisotropy of the dielectric function within a liquid-vapour interface. *Mol. Phys.* 49:1385–1400.
22. Norde, W. 1986. Adsorption of proteins at the solid-liquid interface. *Adv. Colloid Interface Sci.* 25:267–340.
23. MacRitchie, F. 1978. Proteins at interfaces. *Adv. Protein Chem.* 32:283–326.
24. Benjamins, J., A. DeFeijter, M. T. A. Evans, D. E. Graham, and M. C. Phillips. 1975. Dynamic and Static properties of proteins adsorbed at the air/water interface. *Faraday Disc. Chem. Soc.* 59:218–229.
25. Chou, K-C., L. Carlacci, G. M. Maggiora, L. A. Parodi, and M. W. Schulz. 1992. An energy-based approach to packing the 7-helix bundle of bacteriorhodopsin. *Protein Science.* 1:810–827.
26. Ahmed, A. I., R. E. Feeney, D. T. Osuga, and Y. Yeh. 1975. Antifreeze glycoproteins from an Antarctic fish. *J. Biol. Chem.* 250:9, 3344–3347.